

# Ponymation: Learning 3D Animal Motions from Unlabeled Online Videos

Keqiang Sun<sup>1\*</sup>, Dor Litvak<sup>2,3\*†</sup>, Yunzhi Zhang<sup>2</sup>, Hongsheng Li<sup>1</sup>, Jiajun Wu<sup>2†</sup>, Shangzhe Wu<sup>2†</sup>

<sup>1</sup>CUHK MMLab <sup>2</sup>Stanford University <sup>3</sup>UT Austin

[keqiangsun.github.io/projects/ponymation](https://keqiangsun.github.io/projects/ponymation)

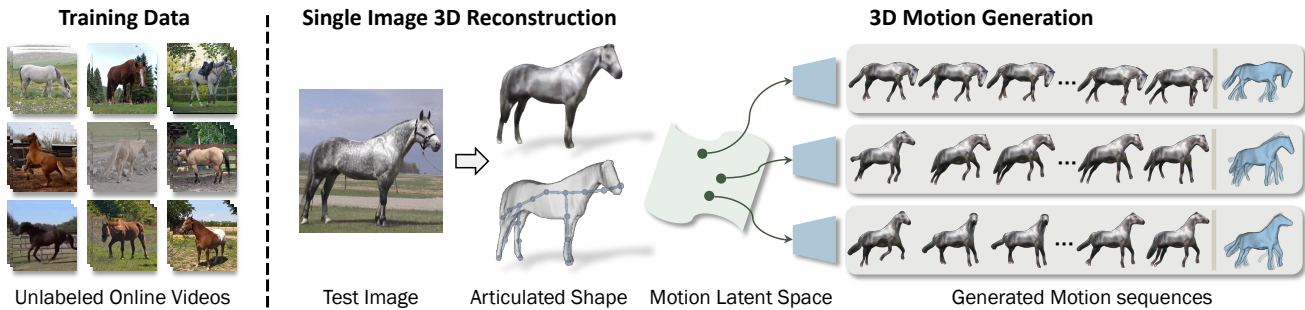


Figure 1. **Learning Articulated 3D Animal Motions from Unlabeled Online Videos.** Given a collection of monocular videos of an animal category obtained from the Internet as training data, our method learns a generative model of the articulated 3D motions together with a category-specific 3D reconstruction model, without relying on any shape templates or pose annotations for training. At inference time, the model takes in a single test image and generates diverse 3D animations by sampling from the learned motion latent space.

## Abstract

We introduce *Ponymation*, a new method for learning a generative model of articulated 3D animal motions from raw, unlabeled online videos. Unlike existing approaches for motion synthesis, our model does not require any pose annotations or parametric shape models for training, and is learned purely from a collection of raw video clips obtained from the Internet. We build upon a recent work, *MagicPony*, which learns articulated 3D animal shapes purely from single image collections, and extend it on two fronts. First, instead of training on static images, we augment the framework with a video training pipeline that incorporates temporal regularizations, achieving more accurate and temporally consistent reconstructions. Second, we learn a generative model of the underlying articulated 3D motion sequences via a spatio-temporal transformer VAE, simply using 2D reconstruction losses without relying on any explicit pose annotations. At inference time, given a single 2D image of a new animal instance, our model reconstructs an articulated, textured 3D mesh, and generates plausible 3D animations by sampling from the learned motion latent space.

\*Equal contribution. †Equal advising.

‡Work was primarily done while Dor Litvak was visiting Stanford.

## 1. Introduction

We share the planet with various kinds of lively animals. Similarly to human beings, they navigate and interact with the physical world, demonstrating various sophisticated motion patterns. In fact, the first film in history, “The Horse in Motion”, was a sequence of photographs capturing a galloping horse, created by Eadweard Muybridge in 1887 [42]. Films only capture sequences of 2D projections of 3D animal movements. Further modeling dynamic animals in 3D is not only useful for numerous mixed reality and content creation applications, but can also provide computational tools for biologists to study animal behaviors.

In this work, we are interested in learning a prior distribution of 3D animal motion patterns with a generative model, simply from a collection of raw video sequences.

Although a lot of efforts have been invested in capturing and modeling 3D human motions using computer vision techniques, significantly less attention has been paid to animals. Existing learning-based approaches require an extensive amount of 3D scans [40, 51, 52], parametric shape models [6, 26, 28, 50, 77], multi-view videos [16, 21, 38], or geometric annotations, such as keypoints [18, 19, 22, 48–50, 57], as supervision for training. Collecting large-scale 3D training data involves specialized capture devices and intensive labor, which can only be justified for specific ob-

jects, like humans, that are of utmost value in applications.

Recent years have seen the rapid development of data-efficient algorithms that can learn 3D objects simply from collections of raw unstructured 2D images [10, 44, 45, 53, 60, 61, 67, 70, 76], without relying on explicit 3D training data or human annotations. At the core of these approaches is a differentiable inverse rendering framework that is trained to explain the training images using a learned canonical 3D model, following an analysis-by-synthesis paradigm. This allows the model to learn various types of natural 3D objects beyond human bodies, including animals in the wild [27, 70, 74, 76]. Despite impressive 3D reconstruction results, these methods reconstruct 3D shapes from individual static images, ignoring the temporal motion dynamics of the underlying objects moving in the physical world. Although a few recent works have used video data for training [68, 72–74], they still either optimize over only a few animal instances [72–74] or obtain a single image reconstruction model [68], without learning a prior distribution of diverse 3D animal motion patterns.

In this work, we would like to learn a generative model that captures the prior distribution of 3D motions of an animal category. Crucially, we study this problem under two challenging conditions. First, unlike existing video synthesis methods [55, 66] that operate on 2D images, we would like to obtain an explicit 3D motion representation, in the form of a 3D mesh and a sequence of articulated 3D poses. This explicit, disentangled 3D representation allows for downstream motion analysis and controllable 3D animation. Second, unlike existing motion synthesis approaches [18, 22, 48, 49], our learning process does not rely on explicit manual supervision, such as keypoints or template shapes, which are often expensive to collect for various animals at scale.

To do this, we capitalize on a recent work, MagicPony [70], which learns articulated 3D models of animal categories from image collections. Instead of relying on explicit annotations for learning 3D shapes, it exploits semantic correspondences distilled from self-supervised image features [8], and learns a category-specific articulated 3D model by matching these noisy correspondences and reconstructing the images. In our work, instead of learning to explain individual static images in 3D, we task the model to explain *sequences of images* with an explicit “4D” representation, *i.e.*, sequences of articulated 3D shapes, through a 3D motion latent space.

Specifically, we design a spatio-temporal transformer VAE that encodes a sequence of images into a latent vector in the motion latent space, and decodes from it a sequence of articulated 3D poses, expressed in the form of bone rotations on an estimated skeleton. In conjunction with a base shape and appearance reconstruction module, the learned 3D motion sequences can be rendered into RGB images, al-

lowing the model to be trained by simply minimizing 2D reconstruction losses on raw RGB video frames, without relying on any explicit pose annotations.

At inference time, given a single image of a new animal instance, our model reconstructs its articulated 3D shape and appearance, and generates diverse plausible 3D animations by sampling from the learned motion latent space. Moreover, this end-to-end video training pipeline also allows us to take advantage of additional temporal signals to learn the 3D shape, leading to more accurate and temporally consistent reconstructions.

To summarize, this paper makes several contributions:

- We propose a new method for learning a generative model of *articulated* 3D animal *motions* from *unlabeled* online videos, without any shape templates or pose annotations;
- We design a spatio-temporal transformer VAE architecture that effectively extracts spatio-temporal motion information from an input video sequence;
- At inference time, the model takes in a single image and generates various realistic 3D animations from the learned motion latent space;
- This video training framework also leads to improved 3D reconstruction accuracy, compared to baseline methods trained on static images.

## 2. Related Work

### 2.1. Learning 3D Animals from Image Collections

While modeling dynamic 3D objects traditionally requires motion capture markers or simultaneous multi-view captures [12, 13, 20], recent learning-based approaches have demonstrated the possibility of learning 3D deformable models simply from raw single-view image collections [17, 27, 34, 36, 67, 70, 76]. Most of these methods require additional geometric supervision besides object masks for training, such as keypoint [27, 35] and viewpoint annotations [14, 46, 56], template shapes [17, 31, 34], semantic correspondences [25, 36, 70, 76], and strong geometric assumptions like symmetries [67, 69]. Among these, MagicPony [70] demonstrates remarkable results in learning articulated 3D animals, such as horses, using only single-view images with object masks and self-supervised image features as training supervision. However, it reconstructs static images individually, ignoring the dynamic motions of the underlying 3D animals behind those images. In this work, we build upon MagicPony, and develop a method for learning a generative model of articulated 3D animal motion sequences simply from a raw monocular video collection.

### 2.2. Deformable Shapes from Monocular Videos

Reconstructing deformable shapes from monocular videos is a long-standing problem in computer vision. Early approaches with Non-Rigid Structure from Motion (NRSfM)

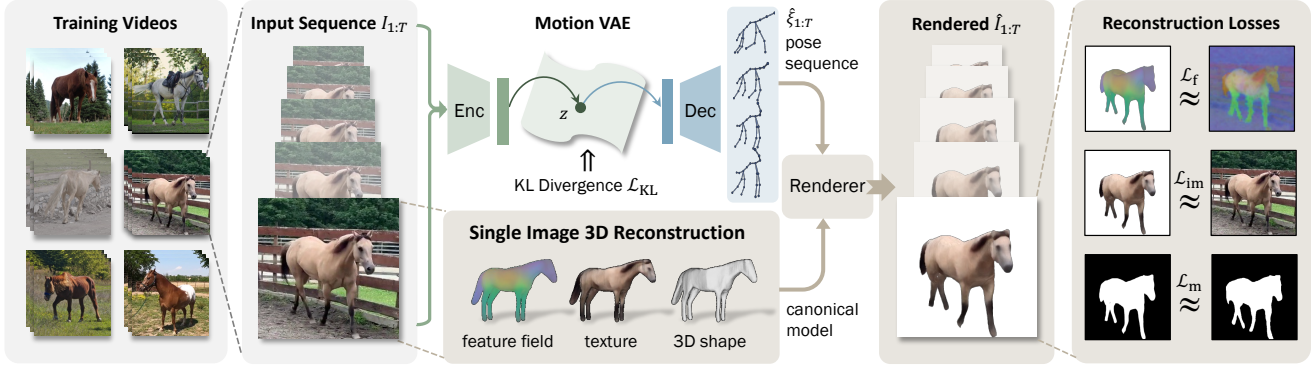


Figure 2. **Training Pipeline.** Our method learns a generative model of articulated 3D motion sequences from a collection of unlabeled monocular videos. During training, the motion VAE encodes an input video sequence  $I_{1:T}$  into a latent code  $z$ , and decodes from it a sequence of articulated 3D poses  $\xi_{1:T}$ . Working in tandem with a single-image 3D reconstruction module, the full pipeline is trained simply using image reconstruction losses with unsupervised image features and segmentation masks obtained from off-the-shelf models.

reconstruct deformable shapes from 2D correspondences, by incorporating heavy constraints on the motion patterns [2, 7, 9, 11, 71]. DynamicFusion [43] further integrates additional depth information from depth sensors. NRSfM pipelines have recently been revived with neural representations. In particular, LASR [72] and its follow-ups [73, 74] optimize deformable 3D shapes over a small set of monocular videos, leveraging 2D optical flows in a heavily engineered optimization procedure. DOVE [68] proposes a learning framework that learns a category-specific 3D model from a large collection of monocular online videos, which allows for single image reconstruction of articulated shapes at test time. However, despite using video data for training, none of these approaches explicitly model the distribution of temporal motion patterns of the objects, which is the focus of this work.

### 2.3. Motion Analysis and Synthesis

Modeling motion patterns of dynamic objects has important applications for both behavior analysis and content generation, and is instrumental to our visual perception system [4]. Computational techniques have been used for decades to study and synthesize human motions [5, 47, 64]. In particular, recent works have explored learning generative models for 3D human motions [1, 18, 22, 39, 41, 48, 49, 57], leveraging parametric human shape models, like SMPL [40], and large-scale human pose annotations [3, 24]. In comparison, much less efforts have been invested in learning animal motions. [23] proposes a hierarchical motion learning framework for animals, but requires costly motion capture data and hardly generalizes to animals in the wild. To sidestep the collection of 3D data, [58] introduces a self-supervised method for discovering and tracking keypoints from videos, but is limited to a 2D representation. Such 2D keypoints could be lifted to 3D, as shown in BKinD-3D [59], but this requires multi-view videos for training. Unlike these prior

works, our motion learning framework does not require any pose annotations or multi-view videos for training, and is trained simply using raw monocular online videos.

## 3. Method

Given a collection of raw video clips of an animal category, such as horses, our goal is to learn a generative model of its articulated 3D motions, which allows us to sample diverse and realistic motion sequences from the learned motion latent space, and animate a new animal instance in 3D given only a single 2D image at test time.

We train this model simply on raw online videos without relying on any explicit pose annotations, building upon the recent work of MagicPony [70]. However, instead of reconstructing static images as in [70], we design a transformer-based motion Variational Auto-Encoder (VAE) that learns a generative model of 3D animal motions by training on videos. Figure 2 gives an overview of the training pipeline.

### 3.1. Overview of MagicPony

Given a collection of static images and automatically obtained instance masks as training data, MagicPony [70] learns a monocular reconstruction model that takes a 2D image as input and predicts the 3D shape, articulated pose, and appearance of the underlying object.

To do this, for each animal category, the model learns a category-specific prior 3D shape using a hybrid SDF-mesh representation [54]. To reconstruct a specific instance in an input image, the model first extracts a feature map and a global feature vector  $(\Phi, \phi) = f_\phi(I)$  using a pre-trained image encoder [8]. With the features, it then estimates a deformation field  $f_{\Delta V}$  that deforms the vertices of the prior mesh accounting for non-structured shape variations (*e.g.*, hair). To account for more controlled deformations caused by the underlying skeletal structure, the model further instantiates a set of bones on the instance mesh, and pre-

dicts an articulated pose  $\hat{\xi} = f_{\xi}(\phi)$ , including a rigid pose  $\hat{\xi}_1 \in SE(3)$  w.r.t. an identity camera pose and the rotations  $\hat{\xi}_b \in SO(3)$  of each bone  $b \in \{2, \dots, B\}$ . The final articulated shape is obtained using a linear blend skinning equation  $g(V, \xi)$  [40]. The model also predicts the appearance  $\hat{A}$  of the object, and the entire pipeline is trained by minimizing reconstruction losses on the rendered images and masks  $(\hat{I}, \hat{M}) = R(\hat{V}, \hat{\xi}, \hat{A})$ , where the pseudo ground-truth is obtained from an off-the-shelf segmentation model [30].

As learning articulated 3D shapes from single-view images is a highly ill-posed inverse task, previous works often rely on additional expensive geometric annotations for training, such as keypoints or template shapes. Instead, MagicPony exploits semantic correspondences distilled from self-supervised image features of DINO-ViT [8]. Specifically, it learns a category-specific feature field, and compares the rendered features with image features extracted from a pre-trained DINO-ViT, which helps register various posed images onto the same canonical model. For more details, please refer to MagicPony [70].

### 3.2. Video Training

Despite reconstructing detailed 3D shapes, MagicPony looks at one single image at a time and ignores the temporal motion dynamics of the underlying animals. This results in sub-optimal reconstructions with discontinuous poses, when applied to video sequences, as illustrated in Figure 3. To enhance temporal consistency for better motion modeling, we introduce a video training pipeline that learns to reconstruct an entire sequence of frames  $\{I_t\}_{t=1}^T$  from a training video clip in one go.

We further incorporate temporal smoothness constraints on the predicted poses  $\hat{\xi}_t$  between consecutive frames, by minimizing the  $\mathcal{L}_2$  distance between the consecutive pose predictions:  $\mathcal{R}_{\text{temp}} = \sum_{t=2}^T \|\hat{\xi}_t - \hat{\xi}_{t-1}\|_2^2$ , including both rigid poses  $\hat{\xi}_{t,1}$  and bone rotations  $\hat{\xi}_{t,2:B}$ .

The training objective hence consists of the reconstruction losses on rendered RGB frames  $\mathcal{L}_{\text{im},t}$ , masks  $\mathcal{L}_{\text{m},t}$ , and DINO features  $\mathcal{L}_{\text{f},t}$ :  $\mathcal{L}_{\text{recon},t} = \mathcal{L}_{\text{im},t} + \lambda_{\text{m}}\mathcal{L}_{\text{m},t} + \lambda_{\text{f}}\mathcal{L}_{\text{f},t}$ . Together with the shape regularizers and viewpoint hypothesis loss inherited from [70] which we summarize by  $\mathcal{R}_{\text{s}}$ , and the proposed temporal smoothness regularizer  $\mathcal{R}_{\text{temp}}$ , the objective of this video training baseline is:

$$\mathcal{L}_{\text{vid}} = \sum_{t=1}^T \mathcal{L}_{\text{recon},t} + \lambda_{\text{s}}\mathcal{R}_{\text{s}} + \lambda_{\text{temp}}\mathcal{R}_{\text{temp}}. \quad (1)$$

Not only does this video training pipeline improve temporal consistency of 3D reconstructions on video sequences, as shown in Figure 3, but also leads to better reconstruction results on static images, as indicated in Table 2, demonstrating the advantages of training on videos. More

importantly, it lays the foundation for modeling the distribution of articulated 3D animal motions, as described next.

### 3.3. Transformer VAE for Motion Synthesis

Based on this disentangled 3D representation, we would like to learn a prior distribution over the animals’ articulated 3D motions. To this end, inspired by prior work on human motion synthesis [48], we adopt a Variational Auto-Encoder (VAE) framework to learn a latent space of articulated motion sequences  $\xi_{1:T}$ . To better model the temporal and spatial structure of the motion, we design a spatio-temporal transformer architecture [65].

Specifically, instead of predicting the pose  $\hat{\xi}_t$  of each input frame  $I_t$  individually, the model encodes the entire sequence of frames  $I_{1:T}$  into the latent space of a VAE, and samples from this space a single latent code  $z$  that predicts the entire sequence of poses  $\hat{\xi}_{1:T}$ . Crucially, unlike prior work that requires 3D pose annotations as input, our model is trained to reconstruct the raw RGB sequences, without any pose annotations for training.

**Sequence Encoding.** To encode a sequence of RGB frames into the VAE latent distribution parameters  $(\hat{\mu}, \hat{\Sigma})$  capturing the motion, we design a pair of spatial and temporal transformer encoders  $E_{\text{s}}$  and  $E_{\text{t}}$ .

Specifically, given each frame  $I_t$  of the input sequence, we first obtain a pose feature by fusing both global image features  $\phi_t$  and local features sampled at the pixel of the bones. Following MagicPony [70], for each bone, we construct a bone-specific feature descriptor  $b$ :  $\nu_{t,b} = (\phi_t, \Phi_t(\mathbf{u}_{t,b}), b, \mathbf{J}_b, \mathbf{u}_{t,b})$ , where  $\mathbf{J}_b$  denotes the 3D location of the bone at rest-pose which projects to the pixel location  $\mathbf{u}_{t,b}$  in the image, and  $\Phi_t(\mathbf{u}_{t,b})$  is the feature vector sampled from the image feature map  $\Phi_t$  at the pixel location  $\mathbf{u}_{t,b}$ .

The spatial transformer encoder  $E_{\text{s}}$  then fuses these feature descriptors into a single feature vector  $\nu_{t,*}$  summarizing the articulated pose of the animal in each frame:

$$\nu_{t,*} = E_{\text{s}}(\nu_{t,2}, \dots, \nu_{t,B}). \quad (2)$$

In practice, we prepend a learnable token to the feature descriptors, and take the first output token of the transformer as the pose feature  $\nu_{t,*}$ . We call this  $E_{\text{s}}$  a *spatial* transformer as it extracts the spatial structural features from each input frame that capture the articulated pose.

Next, we design a second *temporal* transformer encoder  $E_{\text{t}}$  that operates along the temporal dimension and maps the entire sequence of pose features  $\{\nu_{t,*}\}_{t=1}^T$  into the VAE latent space. Similar to the  $E_{\text{s}}$ ,  $E_{\text{t}}$  takes in the pose feature sequence and predicts VAE distribution parameters:

$$(\hat{\mu}, \hat{\Sigma}) = E_{\text{t}}(\nu_{1,*}, \dots, \nu_{T,*}). \quad (3)$$

Using the reparametrization trick [29], we can then sample a single latent code from the Gaussian distribution  $z \sim \mathcal{N}(\hat{\mu}, \hat{\Sigma})$  describing the motion of the entire sequence.



Category	Sequence Num	Duration	Frame Number
Horse	640	28'09"	50,682
Zebra	47	05'27"	9,822
Giraffe	60	04'52"	8,768
Cow	69	07'25"	13,359
Total	816	45'54"	82,631

Table 1. Statistics of the *AnimalMotion* Dataset. To train our motion synthesis model, we collect a new animal video dataset containing a total of 82.6k frames for 4 different categories.

**Motion Decoding.** Symmetric to the encoder, the motion decoder also consists of a temporal decoder  $D_t$  that decodes  $z$  into a sequence of pose features  $z_{1:T}$ , and a spatial decoder  $D_s$  that further decodes each pose feature  $z_t$  to a set of bone rotations  $\hat{\xi}_t$ .

Specifically, we query the temporal transformer decoder  $D_t$  with a sequence of timestamps  $\mathcal{T}$ , and use  $z$  as both key and value tokens to obtain a sequence of pose features:

$$(z_1, \dots, z_T) = D_t(\mathcal{T}, z), \quad \mathcal{T} = (1, \dots, T). \quad (4)$$

Similarly, given each pose feature  $z_t$ , we then query the spatial transformer decoder  $D_s$  with a sequence of bone indices to generate the bone rotations:

$$(\hat{\xi}_{t,2}, \dots, \hat{\xi}_{t,B}) = D_s(\mathcal{B}, z_t), \quad \mathcal{B} = (2, \dots, B). \quad (5)$$

Note that like in MagicPony [70], the rigid pose  $\hat{\xi}_{t,1}$  is predicted by a separate network and not included in this motion VAE, since it is entangled with arbitrary camera poses.

To train the motion VAE, in addition to the reconstruction losses in Equation (1), we also minimize the Kullback–Leibler (KL) divergence between the learned latent distribution and a standard Gaussian distribution:

$$\mathcal{L}_{\text{KL}} = \sum_i -\frac{1}{2} (\log \sigma_i - \sigma_i - \mu_i^2 + 1), \quad (6)$$

where  $\mu_i$  and  $\sigma_i^2$  are elements of the predicted distribution parameters  $\hat{\mu}$  and  $\hat{\Sigma}$ .

**Training Schedule.** As directly learning 3D articulated motion from raw video frames is a challenging task, we train our pipeline in two phases. In the first phase, instead of activating the motion VAE, we use the original single-frame pose prediction network from MagicPony and train with the proposed video-training objective in Equation (1). As 3D shape and pose predictions stabilize after 140 epochs, we swap out the pose network with the motion VAE model in the second phase. To facilitate the training of the VAE, we recycle pose predictions  $\hat{\xi}_t$  from the first phase and use them as pseudo ground-truth to supervise the outputs of the VAE decoder  $\hat{\xi}_t$ , with a teacher loss  $\mathcal{L}_{\text{teacher}} = \sum_{t=1}^T \|\hat{\xi}_t - \hat{\xi}_t\|_2^2$ . The final training objective for the second phase is thus:

$$\mathcal{L} = \mathcal{L}_{\text{vid}} + \lambda_{\text{KL}} \mathcal{L}_{\text{KL}} + \lambda_{\text{teacher}} \mathcal{L}_{\text{teacher}}. \quad (7)$$

Method	Supervision	PCK $\uparrow$	Mask IoU $\uparrow$
Rigid-CSM [32]	kp. + mask	42.1%	-
A-CSM [33]	kp. + mask	44.6%	-
Rigid-CSM [32]	mask	31.2%	-
Dense-Equi [63]	mask	23.3%	-
UMR [37]	mask	24.4%	-
A-CSM [33]	mask	32.9%	-
MagicPony [70]	DINO + mask	42.8%	64.12%
Ponymation (ours)	DINO + mask	<b>48.0%</b>	<b>71.83%</b>

Table 2. Reconstruction Evaluation on PASCAL [15] Dataset. Our method achieves superior reconstruction accuracy compared to a state-of-the-art method MagicPony, and is competitive to methods that require extra supervision from keypoints (denoted as ‘kp.’).

**Inference.** During inference time, we can sample a latent code from the learned motion latent space and generate an arbitrary articulated 3D motion sequence using the motion decoder. Working in conjunction with the single-image 3D reconstruction module, given a single test image of a new animal instance, our final model can reconstruct the 3D shape of the instance and automatically generate 3D animations of it, as illustrated in Figure 4.

## 4. Experiments

### 4.1. Experimental Setup

**Datasets.** To train our model, we collected an *AnimalMotion* dataset consisting of video clips of several quadruped animal categories extracted from the Internet. The statistics of the dataset are summarized in Tab. 1. As pre-processing, we first detect and segment the animal instances in the videos using the off-the-shelf segmentation model of PointRend [30]. To remove occlusion between different instances, we calculated the extent of mask overlap in each frame and exclude crops where two or more masks overlap with each other. We further apply a smoothing kernel to the sequence of bounding boxes to avoid jittering. The non-occluded instances are then cropped and resized to  $256 \times 256$ . The original videos are all at 30fps. To ensure sufficient motion in each sequence, we remove frames with minimal motion (roughly 20%), measured by the magnitude of optical flow estimated from RAFT [62]. To conduct quantitative evaluations and compare with previous methods, we also use PASCAL VOC [15] and APT-36K [75], both of which provide 2D keypoint annotations for each animal in the image.

**Implementation Details.** The encoders and decoders of the motion VAE model ( $E_s$ ,  $E_t$ ,  $D_s$ ,  $D_t$ ) from Sec. 3.3 are implemented as stacked transformers [65] with 4 transformer blocks and a latent dimension of 256, similar to [48]. We apply positional encoding, we followed [48] and used a sinusoidal function. For the rest of the networks de-

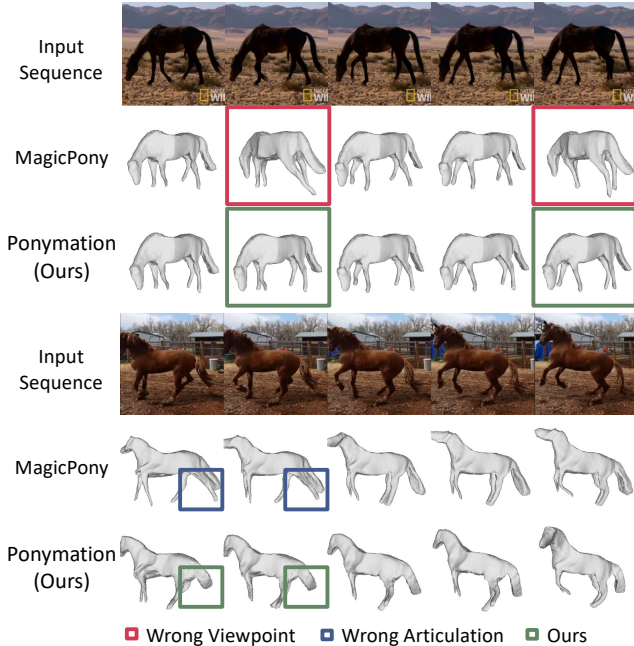


Figure 3. **Comparison of 3D Reconstruction Results with MagicPony [70].** With the video training framework, our method produces temporally coherent and more accurate pose predictions. In comparison, the baseline model of MagicPony often predicts incorrect rigid poses  $\hat{\xi}_{t,1}$  (red boxes), and incorrect bone articulation  $\hat{\xi}_{t,2:B}$  (blue boxes), resulting in inaccurate 3D reconstruction.

scribed in Sec. 3.1, we follow the implementation of MagicPony [70]. We train for 120 epochs in the first phase as described in Sec. 3.3, with  $\lambda_m = 10$ ,  $\lambda_f = 10$ ,  $\lambda_s = 0.1$ ,  $\lambda_{temp} = 1$ . In the second phase, we train the full pipeline end-to-end for another 180 epochs with additionally  $\lambda_{KL} = 0.001$  and  $\lambda_{teacher} = 1$ . The final model is trained on 8 A6000 GPUs for roughly 10 hours for the first training phase and additional 48 hours for the second phase. In our generation model, we empirically set the sequence length  $T$  to 10. For the visualization results, we follow [70] and finetune (only) the appearance network for 100 iterations on each test image which takes less than 10 seconds, as the model struggles to predict detailed textures in a single feed-forward pass. More details are described in the supplementary material.

## 4.2. Single-image 3D Reconstruction

While the main task of this work is learning articulated 3D motions from videos, the underlying 3D representation also enables single-image 3D reconstruction at test time. We first evaluate the quality of the 3D reconstruction, comparing with several existing methods, and analyze motion generation in the next section.

Experiment	APT-36K	PASCAL
	PCK $\uparrow$ / Velocity Err $\downarrow$	PCK@0.1 $\uparrow$ / MIoU $\uparrow$
MP [70]	53.93% / 57.31%	42.8% / 64.12%
MP [70] + AM	57.84% / 49.82%	46.8% / 71.58%
Ponymation (ours)	<b>59.91% / 49.07%</b>	<b>48.0% / 71.83%</b>

Table 3. Reconstruction Evaluation on APT-36K [75] and PASCAL [15]. MP: Magicpony, AM: our AnimalMotion dataset. Both the new AnimalMotion dataset and video training pipeline improve the reconstruction accuracy and temporal consistency.

### 4.2.1 Qualitative Results

Figure 3 compares 3D reconstruction results with the baseline model of MagicPony [70] on video sequences. Although MagicPony predicts a plausible 3D shape in most cases, it tends to produce temporally inconsistent poses, including both viewpoint  $\hat{\xi}_{t,1}$  and bone rotations  $\hat{\xi}_{t,2:B}$ . In comparison, our method leverages the temporal signals in training videos, and produces temporally coherent reconstruction results.

### 4.2.2 Quantitative Evaluations

**Metrics.** Since 3D ground-truth is often unavailable for in-the-wild objects for a direct 3D evaluation, Percentage of Correct Keypoints (**PCK**) has become a commonly used metric on datasets with 2D keypoint annotations [33, 36, 70] for 3D reconstruction evaluation. Given a set of 2D keypoints on a source image, we first map them to the closest vertices on the surface of the reconstructed 3D model, and further project these 3D vertices to the target image in 2D. The Euclidean distance between these projected keypoints and corresponding ground-truth annotations measures the error of the 3D reconstruction results. We calculate the percentage of points with an error smaller than  $0.1 \times \max(h, w)$  and denote it as PCK@0.1, where  $h$  and  $w$  are image height and width, respectively. Another commonly used metric is Mask Intersection over Union (**MIoU**) between the rendered and ground-truth masks, which measures the reconstruction quality in terms of projected 2D silhouettes. In addition, we also measure the temporal consistency of the reconstructions of video frames using the **Velocity Error**, computed as  $\frac{1}{T} \sum_t \|\hat{\delta}_t - \delta_t\| / \delta_t$ , where  $\hat{\delta}_t$  and  $\delta_t$  are the keypoint displacements between consecutive frame for predicted and GT pose sequences respectively.

**Evaluation on PASCAL.** We quantitatively evaluate our method on PASCAL [15], a standard benchmarking dataset for 3D reconstruction, and compare it with prior 3D reconstruction methods, as shown in Table 2. The results from MagicPony are obtained using the code provided by the authors; results for other baselines are taken from A-CSM [33]. Rigid-CSM [32] and A-CSM achieve good performance when trained with extra keypoint supervision, but the results significantly deteriorate when such supervision is not available. Our method builds on top of MagicPony and

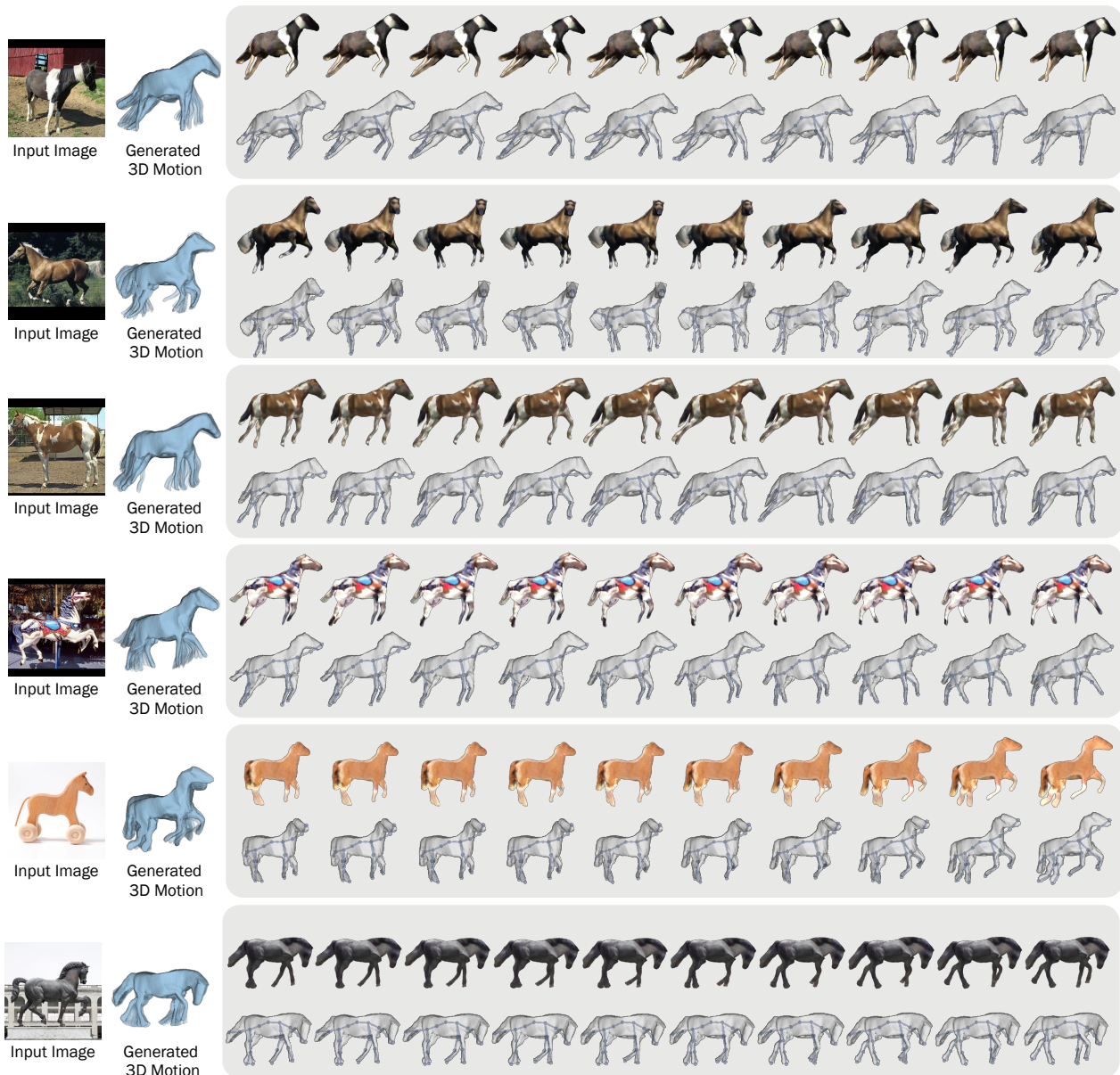


Figure 4. **Test-Time Single-Image 3D Animation.** During test time, our method can animate a novel animal instance in 3D from a single input image. The method can faithfully reconstruct the shape and texture conditioned on the input image, and then render the obtained 3D representation with plausible motion sampled from the motion latent space. The first row within each gray box shows textured animation, and the second row shows corresponding 3D shapes overlapped with predicted bone articulation.

additionally benefits from the temporal signals by training on videos, with an improved PCK@0.1 score from 42.8% to 48.0%, and a mask IoU from 64.12% to 71.83%, compared to the MagicPony baseline. Overall, our method achieves performance competitive with keypoint-supervised methods, and outperforms all existing unsupervised methods by a significant margin.

We also conduct ablation studies to analyze the effects of each component and report the results in Table 3. In par-

ticular, training on our new Animal Motion dataset leads to significant performance boost, and combined with the temporal smooth regularization, the final model demonstrates further improvements.

**Evaluation on APT-36K.** To better understand the performance on video reconstructions, we present a quantitative evaluation on APT-36K [75], an animal video dataset with 2D keypoint annotations. We use the 81 video clips of horses with a total of 1207 frame (each frame may con-



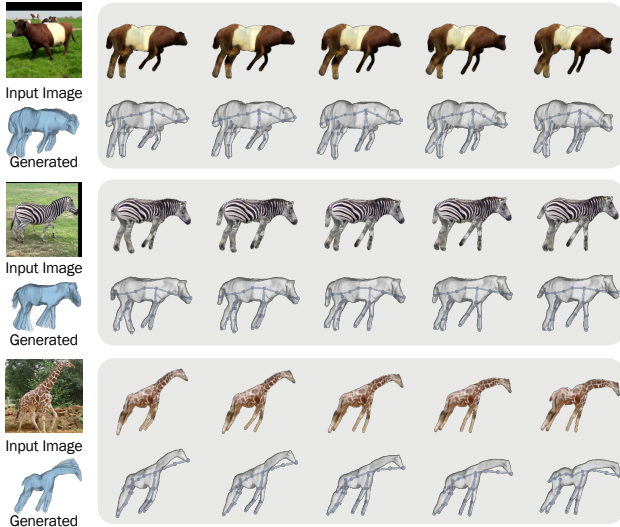


Figure 5. **Motion Synthesis Results on More Categories.** Our method can be trained on video data from different categories such as corws, zebras, and giraffes, and generate plausible motion sequences. The learned motions appear to be specific to the animal category, such as the third example, where the generated neck motion is more prominent for giraffes than others.

tain multiple instances). Each horse is annotated with 17 keypoints. We use the same pre-processing procedure as in the training set to crop all the instances, and only keep instances that have full 17 keypoints annotations. This results in a total 92 sequences containing 965 frames overall, which we use to evaluate the sequence reconstruction performance. Since the skeleton automatically discovered by our model is different from the 17 keypoints annotated in APT-36K, we map our predicted joints to the GT keypoints by simply optimizing a linear transformation, following [27], and report PCK@0.1 in Tab. 3. Overall, our video training pipeline leads to considerable improvements over the MagicPony baselines.

### 4.3. 3D Motion Generation

#### 4.3.1 Qualitative Results

After training, samples from the motion latent space can generate diverse, realistic 3D motion sequences, which can be rendered with textured meshes reconstructed from a single 2D image, as shown in Figure 4. It also generalizes to horse-like artifacts, such as carousel horses, which the model has never seen during training. Beside horses, the model can be trained on a wide range of categories, including giraffes, zebras and cows, as shown in Figure 5. Because the datasets for these categories are limited in size and diversity, similarly to [70], in the first phase of the training, we fine-tune from the model trained on horses. With the proposed training framework, our model is able to capture a category-specific prior distribution of articulated 3D mo-

Experiment	MCD ↓
MP + VAE	38.77
MP + AM + VAE	38.12
Final Model (MP + AM + TS + VAE)	<b>38.03</b>

Table 4. Motion Chamfer Distance (MCD) on APT-36K [75] for motion generation evaluation. MP: Magicpony, AM: AnimalMotion Dataset, TS: Temporal Smoothness.

tions, and render realistic animation results on a variety of animal categories. Additional 3D animation results are provided in the supplementary video.

#### 4.3.2 Quantitative Evaluation

To assess the quality of our generated motion sequences, for the lack of ground-truth animal motion capture data, we introduce a proxy metric, bi-directional Motion Chamfer Distance (MCD), computed between a set of generated motion sequences projected to 2D and the annotated keypoint sequences in APT-36K [75]. Specifically, we randomly sample from the learned motion latent space and generate 1, 400 motion samples, each consisting of 10 frames of articulated poses projected to 2D. For the pose in each frame, we apply the same mapping function described previously to align with the the GT keypoints. To compute MCD, each GT keypoint *sequence* in the test set, we find the closest generated motion *sequence* measured by keypoint MSE averaged across all frames, and vice versa for each generated sequence. In essence, MCD measures the fidelity of motion generation by comparing the distribution of generated motions to that of the real motion sequences in videos. We compare the results generated by different variants of the model in Table 4. In summary, when combined with the motion VAE pipeline, training on the new video dataset with the temporal constraints improve the fidelity of the generated motion sequences.

## 5. Conclusions

We have presented a generative model for learning the distribution of articulated 3D animal motions from raw Internet videos, without relying on any pose annotations or shape templates. We proposed a transformer-based motion VAE model that exploits the temporal and spatial structure of an explicit underlying representation of articulated 3D motions in a video training framework. Experimental results show that the proposed method captures a plausible distribution of 3D animal motions for several animal categories. This allows us to reconstruct a 3D model and automatically generate 3D animations of a new animal instance, from just a single 2D image at test time.

**Acknowledgments.** We are grateful to Zizhang Li, Feng Qiu and Ruining Li for insightful discussions.



## References

- [1] Hyemin Ahn, Timothy Ha, Yunho Choi, Hwiyeon Yoo, and Songhwai Oh. Text2action: Generative adversarial synthesis from language to action. In *ICRA*, pages 1–5, 2018. 3
- [2] Ijaz Akhter, Yaser Sheikh, Sohaib Khan, and Takeo Kanade. Nonrigid structure from motion in trajectory space. In *NeurIPS*, 2008. 3
- [3] Mykhaylo Andriluka, Leonid Pishchulin, Peter Gehler, and Bernt Schiele. 2d human pose estimation: New benchmark and state of the art analysis. In *CVPR*, 2014. 3
- [4] Norman Badler. *Temporal Scene Analysis: Conceptual Descriptions of Object Movements*. PhD thesis, Queensland University of Technology, 1975. 3
- [5] Norman I Badler, Cary B Phillips, and Bonnie Lynn Webber. *Simulating Humans: Computer Graphics, Animation, and Control*. Oxford University Press, 1993. 3
- [6] Federica Bogo, Angjoo Kanazawa, Christoph Lassner, Peter Gehler, Javier Romero, and Michael J. Black. Keep it SMPL: Automatic estimation of 3D human pose and shape from a single image. In *ECCV*, 2016. 1
- [7] Christoph Bregler, Aaron Hertzmann, and Henning Biermann. Recovering non-rigid 3d shape from image streams. In *CVPR*, 2000. 3
- [8] Mathilde Caron, Hugo Touvron, Ishan Misra, Hervé Jégou, Julien Mairal, Piotr Bojanowski, and Armand Joulin. Emerging properties in self-supervised vision transformers. In *ICCV*, 2021. 2, 3, 4
- [9] Thomas J. Cashman and Andrew W. Fitzgibbon. What shape are dolphins? building 3d morphable models from 2d images. *IEEE TPAMI*, 2012. 3
- [10] Eric Chan, Marco Monteiro, Petr Kellnhofer, Jiajun Wu, and Gordon Wetzstein. pi-GAN: Periodic implicit generative adversarial networks for 3d-aware image synthesis. In *CVPR*, 2021. 2
- [11] Yuchao Dai, Hongdong Li, and Mingyi He. A simple prior-free method for non-rigid structure-from-motion factorization. In *CVPR*, 2012. 3
- [12] Edilson de Aguiar, Carsten Stoll, Christian Theobalt, Naveed Ahmed, Hans-Peter Seidel, and Sebastian Thrun. Performance capture from sparse multi-view video. *ACM TOG*, 2008. 2
- [13] Paul Debevec. The light stages and their applications to photoreal digital actors. In *SIGGRAPH Asia*, 2012. 2
- [14] Shivam Duggal and Deepak Pathak. Topologically-aware deformation fields for single-view 3d reconstruction. *CVPR*, 2022. 2
- [15] Mark Everingham, SM Ali Eslami, Luc Van Gool, Christopher KI Williams, John Winn, and Andrew Zisserman. The pascal visual object classes challenge: A retrospective. *IJCV*, 111:98–136, 2015. 5, 6
- [16] Xiangjun Gao, Jialong Yang, Jongyoo Kim, Sida Peng, Zicheng Liu, and Xin Tong. Mps-nerf: Generalizable 3d human rendering from multiview images. *IEEE TPAMI*, 2022. 1
- [17] Shubham Goel, Angjoo Kanazawa, and Jitendra Malik. Shape and viewpoints without keypoints. In *ECCV*, 2020. 2
- [18] Chuan Guo, Xinxin Zuo, Sen Wang, Shihao Zou, Qingyao Sun, Annan Deng, Minglun Gong, and Li Cheng. Action2motion: Conditioned generation of 3d human motions. In *ACM MM*, 2020. 1, 2, 3
- [19] Ikhsanul Habibie, Daniel Holden, Jonathan Schwarz, Joe Yearsley, and Taku Komura. A recurrent variational autoencoder for human motion synthesis. In *BMVC*, 2017. 1
- [20] Richard Hartley and Andrew Zisserman. *Multiple View Geometry in Computer Vision*. Cambridge University Press, ISBN: 0521540518, second edition, 2004. 2
- [21] Yannan He, Anqi Pang, Xin Chen, Han Liang, Minye Wu, Yuexin Ma, and Lan Xu. Challengcap: Monocular 3d capture of challenging human performances using multi-modal references. In *CVPR*, pages 11400–11411, 2021. 1
- [22] Gustav Eje Henter, Simon Alexanderson, and Jonas Beskow. Moglow: Probabilistic and controllable motion synthesis using normalising flows. *ACM TOG*, 39(6):1–14, 2020. 1, 2, 3
- [23] Kang Huang, Yaning Han, Ke Chen, Hongli Pan, Gaoyang Zhao, Wenling Yi, Xiaoxi Li, Siyuan Liu, Pengfei Wei, and Liping Wang. A hierarchical 3d-motion learning framework for animal spontaneous behavior mapping. *Nature communications*, 12(1):2784, 2021. 3
- [24] Catalin Ionescu, Dragos Papava, Vlad Olaru, and Cristian Sminchisescu. Human3.6m: Large scale datasets and predictive methods for 3d human sensing in natural environments. *IEEE TPAMI*, 36(7):1325–1339, 2014. 3
- [25] Tomas Jakab, Ruining Li, Shangzhe Wu, Christian Rupprecht, and Andrea Vedaldi. Farm3D: Learning articulated 3D animals by distilling 2D diffusion. In *3DV*, 2024. 2
- [26] Angjoo Kanazawa, Michael J. Black, David W. Jacobs, and Jitendra Malik. End-to-end recovery of human shape and pose. In *CVPR*, 2018. 1
- [27] Angjoo Kanazawa, Shubham Tulsiani, Alexei A. Efros, and Jitendra Malik. Learning category-specific mesh reconstruction from image collections. In *ECCV*, 2018. 2, 8
- [28] Angjoo Kanazawa, Jason Y. Zhang, Panna Felsen, and Jitendra Malik. Learning 3d human dynamics from video. In *CVPR*, 2019. 1
- [29] Diederik P Kingma and Max Welling. Auto-encoding variational bayes. *arXiv preprint arXiv:1312.6114*, 2013. 4
- [30] Alexander Kirillov, Yuxin Wu, Kaiming He, and Ross Girshick. PointRend: Image segmentation as rendering. In *CVPR*, 2020. 4, 5
- [31] Filippos Kokkinos and Iasonas Kokkinos. To the point: Correspondence-driven monocular 3d category reconstruction. In *NeurIPS*, 2021. 2
- [32] Nilesh Kulkarni, Abhinav Gupta, and Shubham Tulsiani. Canonical surface mapping via geometric cycle consistency. In *ICCV*, 2019. 5, 6
- [33] Nilesh Kulkarni, Abhinav Gupta, David F Fouhey, and Shubham Tulsiani. Articulation-aware canonical surface mapping. In *Proceedings of the IEEE/CVF Conference on Computer Vision and Pattern Recognition*, pages 452–461, 2020. 5, 6
- [34] Nilesh Kulkarni, Abhinav Gupta, David F. Fouhey, and Shubham Tulsiani. Articulation-aware canonical surface mapping. In *CVPR*, 2020. 2

- [35] Xueting Li, Sifei Liu, Shalini De Mello, Kihwan Kim, Xiaolong Wang, Ming-Hsuan Yang, and Jan Kautz. Online adaptation for consistent mesh reconstruction in the wild. In *NeurIPS*, 2020. 2
- [36] Xueting Li, Sifei Liu, Kihwan Kim, Shalini De Mello, Varun Jampani, Ming-Hsuan Yang, and Jan Kautz. Self-supervised single-view 3d reconstruction via semantic consistency. In *ECCV*, 2020. 2, 6
- [37] Xueting Li, Sifei Liu, Kihwan Kim, Shalini De Mello, Varun Jampani, Ming-Hsuan Yang, and Jan Kautz. Self-supervised single-view 3d reconstruction via semantic consistency. In *ECCV*, 2020. 5
- [38] Zhengqi Li, Tali Dekel, Forrester Cole, Richard Tucker, Noah Snavely, Ce Liu, and William T Freeman. Learning the depths of moving people by watching frozen people. In *CVPR*, pages 4521–4530, 2019. 1
- [39] Xiaoyu Lin and Mohamed R. Amer. Human motion modeling using dvgs. *arXiv preprint arXiv:1804.10652*, 2018. 3
- [40] Matthew Loper, Naureen Mahmood, Javier Romero, Gerard Pons-Moll, and Michael J Black. SMPL: A skinned multi-person linear model. *ACM TOG*, 2015. 1, 3, 4
- [41] Matthias Minderer, Chen Sun, Ruben Villegas, Forrester Cole, Kevin P Murphy, and Honglak Lee. Unsupervised learning of object structure and dynamics from videos. *NeurIPS*, 32, 2019. 3
- [42] Eadweard Muybridge. The horse in motion, 1887. 1
- [43] Richard A. Newcombe, Dieter Fox, and Steven M. Seitz. DynamicFusion: Reconstruction and tracking of non-rigid scenes in real-time. In *CVPR*, 2015. 3
- [44] Thu Nguyen-Phuoc, Chuan Li, Lucas Theis, Christian Richardt, and Yong-Liang Yang. HoloGAN: Unsupervised learning of 3d representations from natural images. In *ICCV*, 2019. 2
- [45] Michael Niemeyer and Andreas Geiger. GIRAFFE: Representing scenes as compositional generative neural feature fields. In *CVPR*, 2021. 2
- [46] Michael Niemeyer, Lars Mescheder, Michael Oechsle, and Andreas Geiger. Differentiable volumetric rendering: Learning implicit 3d representations without 3d supervision. In *CVPR*, 2020. 2
- [47] Dirk Ormoneit, Michael Black, Trevor Hastie, and Hedvig Kjellström. Representing cyclic human motion using functional analysis. *Image and Vision Computing*, 23:1264–1276, 2005. 3
- [48] Mathis Petrovich, Michael J. Black, and Gül Varol. Action-conditioned 3D human motion synthesis with transformer VAE. In *ICCV*, 2021. 1, 2, 3, 4, 5
- [49] Mathis Petrovich, Michael J Black, and Gül Varol. Temos: Generating diverse human motions from textual descriptions. In *ECCV*, 2022. 2, 3
- [50] Jingtian Piao, Keqiang Sun, Quan Wang, Kwan-Yee Lin, and Hongsheng Li. Inverting generative adversarial renderer for face reconstruction. In *Proceedings of the IEEE/CVF Conference on Computer Vision and Pattern Recognition*, pages 15619–15628, 2021. 1
- [51] Shunsuke Saito, Zeng Huang, Ryota Natsume, Shigeo Morishima, Angjoo Kanazawa, and Hao Li. Pifu: Pixel-aligned implicit function for high-resolution clothed human digitization. In *ICCV*, 2019. 1
- [52] Shunsuke Saito, Tomas Simon, Jason Saragih, and Hanbyul Joo. Pifuhd: Multi-level pixel-aligned implicit function for high-resolution 3d human digitization. In *CVPR*, 2020. 1
- [53] Katja Schwarz, Yiyi Liao, Michael Niemeyer, and Andreas Geiger. GRAF: Generative radiance fields for 3d-aware image synthesis. In *NeurIPS*, 2020. 2
- [54] Tianchang Shen, Jun Gao, Kangxue Yin, Ming-Yu Liu, and Sanja Fidler. Deep marching tetrahedra: a hybrid representation for high-resolution 3d shape synthesis. In *NeurIPS*, 2021. 3
- [55] Uriel Singer, Adam Polyak, Thomas Hayes, Xi Yin, Jie An, Songyang Zhang, Qiyuan Hu, Harry Yang, Oron Ashual, Oran Gafni, Devi Parikh, Sonal Gupta, and Yaniv Taigman. Make-a-video: Text-to-video generation without text-video data. In *ICLR*, 2023. 2
- [56] Vincent Sitzmann, Michael Zollhöfer, and Gordon Wetzstein. Scene representation networks: Continuous 3d-structure-aware neural scene representations. In *NeurIPS*, 2019. 2
- [57] Sebastian Starke, Ian Mason, and Taku Komura. Deepphase: Periodic autoencoders for learning motion phase manifolds. *ACM Trans. Graph.*, 41(4), 2022. 1, 3
- [58] Jennifer J Sun, Serim Ryou, Roni Goldshmid, Brandon Weissbourd, John Dabiri, David J Anderson, Ann Kennedy, Yisong Yue, and Pietro Perona. Self-supervised keypoint discovery in behavioral videos. *arXiv preprint arXiv:2112.05121*, 2021. 3
- [59] Jennifer J Sun, Pierre Karashchuk, Amil Dravid, Serim Ryou, Sonia Fereidooni, John Tuthill, Aggelos Katsaggelos, Bingni W Brunton, Georgia Gkioxari, Ann Kennedy, et al. Bkind-3d: Self-supervised 3d keypoint discovery from multi-view videos. *arXiv preprint arXiv:2212.07401*, 2022. 3
- [60] Keqiang Sun, Shangzhe Wu, Zhaoyang Huang, Ning Zhang, Quan Wang, and Hongsheng Li. Controllable 3d face synthesis with conditional generative occupancy fields. In *Advances in Neural Information Processing Systems*, 2022. 2
- [61] Keqiang Sun, Shangzhe Wu, Ning Zhang, Zhaoyang Huang, Quan Wang, and Hongsheng Li. Cgof++: Controllable 3d face synthesis with conditional generative occupancy fields. *IEEE Transactions on Pattern Analysis and Machine Intelligence*, 2023. 2
- [62] Zachary Teed and Jia Deng. Raft: Recurrent all-pairs field transforms for optical flow. In *Computer Vision—ECCV 2020: 16th European Conference, Glasgow, UK, August 23–28, 2020, Proceedings, Part II 16*, pages 402–419. Springer, 2020. 5
- [63] James Thewlis, Hakan Bilen, and Andrea Vedaldi. Unsupervised learning of object frames by dense equivariant image labelling. *NeurIPS*, 30, 2017. 5
- [64] Raquel Urtasun, David J. Fleet, and Neil D. Lawrence. Modeling human locomotion with topologically constrained latent variable models. In *Human Motion – Understanding*,

- Modeling, Capture and Animation*, pages 104–118, Berlin, Heidelberg, 2007. Springer Berlin Heidelberg. 3
- [65] Ashish Vaswani, Noam Shazeer, Niki Parmar, Jakob Uszkoreit, Llion Jones, Aidan N Gomez, Łukasz Kaiser, and Illia Polosukhin. Attention is all you need. In *NeurIPS*, 2017. 4, 5
- [66] Yunbo Wang, Mingsheng Long, Jianmin Wang, Zhifeng Gao, and Philip S Yu. Predrnn: Recurrent neural networks for predictive learning using spatiotemporal lstms. *NeurIPS*, 30, 2017. 2
- [67] Shangzhe Wu, Christian Rupprecht, and Andrea Vedaldi. Unsupervised learning of probably symmetric deformable 3D objects from images in the wild. In *CVPR*, 2020. 2
- [68] Shangzhe Wu, Tomas Jakab, Christian Rupprecht, and Andrea Vedaldi. DOVE: Learning deformable 3d objects by watching videos. *arXiv preprint arXiv:2107.10844*, 2021. 2, 3
- [69] Shangzhe Wu, Ameesh Makadia, Jiajun Wu, Noah Snavely, Richard Tucker, and Angjoo Kanazawa. De-rendering the world’s revolutionary artefacts. In *CVPR*, 2021. 2
- [70] Shangzhe Wu, Ruining Li, Tomas Jakab, Christian Rupprecht, and Andrea Vedaldi. MagicPony: Learning articulated 3d animals in the wild. In *CVPR*, 2023. 2, 3, 4, 5, 6, 8
- [71] Jing Xiao, Jin xiang Chai, and Takeo Kanade. A closed-form solution to non-rigid shape and motion recovery. In *ECCV*, 2004. 3
- [72] Gengshan Yang, Deqing Sun, Varun Jampani, Daniel Vlasic, Forrester Cole, Huiwen Chang, Deva Ramanan, William T. Freeman, and Ce Liu. LASR: Learning articulated shape reconstruction from a monocular video. In *CVPR*, 2021. 2, 3
- [73] Gengshan Yang, Deqing Sun, Varun Jampani, Daniel Vlasic, Forrester Cole, Ce Liu, and Deva Ramanan. ViSER: Video-specific surface embeddings for articulated 3d shape reconstruction. In *NeurIPS*, 2021. 3
- [74] Gengshan Yang, Minh Vo, Neverova Natalia, Deva Ramanan, Vedaldi Andrea, and Joo Hanbyul. BANMo: Building animatable 3d neural models from many casual videos. In *CVPR*, 2022. 2, 3
- [75] Yuxiang Yang, Junjie Yang, Yufei Xu, Jing Zhang, Long Lan, and Dacheng Tao. APT-36K: A large-scale benchmark for animal pose estimation and tracking. In *NeurIPS Dataset and Benchmark Track*, 2022. 5, 6, 7, 8, 12
- [76] Chun-Han Yao, Wei-Chih Hung, Michael Rubinstein, Yuanzhen Lee, Varun Jampani, and Ming-Hsuan Yang. Lassie: Learning articulated shape from sparse image ensemble via 3d part discovery. In *NeurIPS*, 2022. 2
- [77] Jason Y Zhang, Panna Felsen, Angjoo Kanazawa, and Jitendra Malik. Predicting 3d human dynamics from video. In *ICCV*, 2019. 1

# Appendices

## A. Additional Qualitative Results

**Results on Horses.** More motion synthesis results for horses are shown in Figure 6. Please refer to the supplementary.mp4 for more animation results. As shown in the video, by sampling the learned motion latent VAE, we can generate diverse motion patterns such as eating with the head bending towards the ground, walking with legs moving alternatively, and jumping where front legs are lifted.

We trained our VAE model with a sequence length of 10 frames. To produce longer motion sequences as demonstrated in the video, we first sample 2 latent codes to generate 2 motion sequences, each comprising 10 frames. We then optimize 1 additional transition motion latents by encouraging the poses of the first frame and the last frame to be consistent with the last frame and the first frame of two consecutive sequences previously generated.

**Results on Other Categories.** We include more qualitative results for giraffes, zebras and cows in Figure 7. For different animal categories, our model automatically learns different motion priors. For example, in the synthesized results, it is more common for horses to raise their hooves, while neck movements are more typical for giraffes.

## B. Implementation Details

**Architecture.** As explained in the paper, we adopt a spatio-temporal transformer architecture for sequence feature encoding and motion decoding. As illustrated in Tab. 5, we use the 4-layer transformer to implement the spatial and temporal transformer encoder  $E_s$ ,  $E_t$  and decoder  $D_s$ ,  $D_t$ . Given the DINO feature of the input image, we first concatenate the bone position as Positional Encoding to obtain the feature with shape (JointNum, FrameNum, FeatureDim) =  $(20 \times 10 \times 640)$ . Then we adjust the feature dimension to 256 with a simple Linear layer and we concatenate a Bone-FeatureQuery. We employ the 4-layer  $E_s$  to query the global feature of the 20 joints and  $E_t$  to obtain the global feature for all the 10 frames, represented by a mean value  $\mu$  and variance  $\sigma$ . With the output  $\mu$  and  $\sigma$ , we reparameterize a latent code  $z$ , which is first decoded in temporal dimension by  $D_t$  and in spatial dimension by  $D_s$ . The recovered spatio-temporal feature is eventually converted to the articulation value of each joint at each time step.

## C. Ablation Study

**Sequence Length.** We conducted experiments to understand the effect of different sequence lengths during training (20 and 50 frames). To evaluate the longer motion sequences generated by these variants in a fair comparison, we

Operation	Output Size
Positional Encoding	$20 \times 10 \times 640$
Linear(640, 256)	$20 \times 10 \times 256$
Concat BoneFeatQuery	$21 \times 10 \times 256$
TransformerLayer $\times 4$	$1 \times 10 \times 256$
Reshape	$10 \times 1 \times 256$
Concat muQuery and SigmaQuery	$12 \times 1 \times 256$
Positional Encoding	$12 \times 1 \times 256$
TransformerLayer $\times 4$	$2 \times 1 \times 256$
<hr/>	
Reparameterization	$1 \times 1 \times 256$
<hr/>	
TransformerLayer $\times 4$	$10 \times 1 \times 256$
Reshape	$1 \times 10 \times 256$
TransformerLayer $\times 4$	$20 \times 10 \times 256$
Reshape	$10 \times 20 \times 256$
Linear(256, 3)	$10 \times 20 \times 3$

Table 5. Architecture of the proposed spatio-temporal transformer VAE.

Frame Num	10	20	50
MCD $\downarrow$	<b>38.03</b>	38.25	39.25

Table 6. Motion Chamfer Distance (MCD) on APT-36K [75] for motion generation evaluation.

divide them into consecutive sub-sequences of 10 frames. We use the same metric as introduced in the main paper, the Motion Chamfer Distance (MCD) calculated between generated sequences and the annotated sequences in the APT-36K dataset [75]. For the longer sequences, we average out the MCD scores for all sub-sequences. The results are presented in Table 6.

Upon analyzing the results, we observed that the generated sequences still look plausible as the sequence length increases from 10 to 20. However, a notable degradation in performance can be seen as the sequence length increases to 50. This could potentially be attributed to limited capacity of the motion VAE model as well as the limited size of the training dataset. For our final model, we set the sequence length to 10 which tends to yield the most satisfactory results with a reasonable training efficiency.

**Spatio-Temporal Transformer Architecture.** We conduct an ablation study to verify the effectiveness of the proposed spatio-temporal transformer architecture. In particular, we remove the spatial transformer encoder and decoder,  $E_s$  and  $D_s$  and report the results in row 2 of Tab. 7. Specifically, instead of using the spatial transformer encoder  $E_s$  to fuse bone-specific local image features before passing them to the temporal transformer encoder  $E_t$ , we directly feed the global image features  $\{\phi_1, \dots, \phi_T\}$  into the temporal encoder. Similarly, we also remove the spatial decoder  $D_s$ , and directly decode a fixed set of bone rotations from the



	Method Name	PCK@0.1	Mask IoU
1	Final (with ST-Transformer)	37.63%	62.03%
2	with S-Transformer	33.44%	58.89%
3	without motion VAE	44.30%	66.72%

Table 7. Ablation study on the architecture of the motion VAE model.

	Method Name	PCK@0.1	Mask IoU
1	$\lambda_{\text{KL}} = 0.01$	33.58%	59.85%
2	$\lambda_{\text{KL}} = 0.001$	<b>37.63%</b>	<b>62.03%</b>
3	$\lambda_{\text{KL}} = 0.0001$	35.75%	61.11%

Table 8. Ablation study on the weight of the KL divergence loss  $\lambda L_{\text{KL}}$ .

temporal transformer decoder  $D_t$ .

Compared to the final model with spatio-temporal transformer architectures in row 1 of Tab. 7, the variant without spatial transformer results in less accurate reconstructions, and hence lower scores on the metrics. This confirms the effectiveness of the proposed spatial transformer in extracting motion-specific spatial information from the images.

**KL Loss Weight.** To train the motion VAE, in addition to the reconstruction losses, we also use the Kullback–Leibler (KL) divergence loss in Equation (6) in the main paper. We conducted an ablation study on its weight  $\lambda_{\text{KL}}$  to assess its impact on the overall video reconstruction performance. As shown in Table 8,  $\lambda_{\text{KL}} = 0.001$  achieves the best reconstruction performance and is used in all experiments from the main paper.

## D. Limitations

Despite promising results, this model can still be improved on several fronts. Most critically, the articulated motion is learned on top of a fixed bone topology, which is defined with strong heuristics, *e.g.* the number of legs, and may not generalize across distant animal species. Automatically discovering the articulation structure jointly with the video training will be an interesting future direction.



Figure 6. **Additional Motion Synthesis Results on Horses.** Conditioned on an input image, which can be either a real photo or a painting of a horse, our model can generate realistic 4D animations of the instance. See the supplementary video for better visualizations.



Figure 7. **Additional Motion Synthesis Results for Other Categories.** Our model can also be trained on other categories besides horses, and generates realistic motion sequences.